

Probing the Schwarzschild black hole immersed in a dark matter halo through astrophysical tests

Tursunali Xamidov,^{1,*} Sanjar Shaymatov,^{1,2,3,†} Qiang Wu,^{2,4,‡} and Tao Zhu^{2,4,§}

¹ Institute of Fundamental and Applied Research,

National Research University TIIAME, Kori Niyoziy 39, Tashkent 100000, Uzbekistan

² Institute for Theoretical Physics & Cosmology, Zhejiang University of Technology, Hangzhou 310023, China

³ University of Tashkent for Applied Sciences, Str. Gavhar 1, Tashkent 100149, Uzbekistan

⁴ United Center for Gravitational Wave Physics (UCGWP),
Zhejiang University of Technology, Hangzhou 310023, China

(Dated: July 18, 2025)

We investigate a recently derived Schwarzschild-like black hole (BH) immersed in a Dehnen-type $(\alpha, \beta, \gamma) = (1, 4, 5/2)$ dark matter (DM) halo. We obtain constraints on the two model parameters, i.e., the halo core radius r_s and the DM density parameter ρ_s in both the weak and the strong field regimes. In the weak field, we model test particle geodesics and match the predicted perihelion shift to Mercury (Solar System) and the orbit of the S2 star data. We obtain upper limits on r_s and ρ_s and highlight that the DM halo effects become observable only around supermassive BHs. In the strong field, we analyse twin high frequency quasiperiodic oscillations (QPOs) from four microquasars (e.g., GRO J1655-40, GRS 1915+105, XTE J1859+226, and XTE J1550-564). Because QPO frequencies depend only on the local spacetime curvature, they can serve as a probe of halo-induced deviations from general relativity. Our MCMC analysis produces posterior distributions for model parameters, revealing close agreement between the theoretical QPO frequencies and the observations for GRS 1915+105 and GRO J1655-40. The same analysis also yielded best-fit values and upper bounds for each parameter. Our combined geodesic and QPO analysis demonstrates that timelike orbits and epicyclic oscillations can act as sensitive probes of DM halos around BHs, offering a pathway to distinguish Dehnen-type profiles from alternative DM distributions in future analysis and observations.

I. INTRODUCTION

Black hole (BH) astrophysics has entered a precision era. Horizon-scale images of M87* and Sgr A* captured by the Event Horizon Telescope [1, 2], together with the steadily growing set of gravitational wave (GW) detections [3, 4], now allow the strong-gravity regime to be studied with direct data rather than purely through theory. In theoretical models, black holes are often treated as isolated objects, yet in reality they continuously interact with the surrounding baryonic medium. Astronomical observations further reveal an additional, non-baryonic component - dark matter - that accounts for roughly 27 % of the Universe's total mass-energy content, and thus also plays a crucial role in cosmic structure and evolution [5]. Because DM neither emits, absorbs, nor scatters electromagnetic radiation, it remains invisible and can be traced only through the gravity it exerts. Its fingerprints first emerged in the galactic rotation curves, where stars orbit far faster than luminous matter alone can support [6]. Similar mass discrepancies appear in the gravitational lensing maps of galaxy clusters, whose deflection angles exceed general-relativistic predictions based on visible mass [7, 8].

Although plenty of evidence supports the existence of dark matter (DM), its non-gravitational properties remain unknown. Various theoretical models have been proposed: some treat DM as weakly interacting massive particles (WIMPs) coupling via gravity and the weak nuclear force, while others invoke alternative candidates such as axions or sterile neutrinos [9–12]. Because the influence of DM is very weak, we can detect it only in very massive systems. Therefore, studying DM in strong gravitational fields is extremely important. In most models of a black hole-dark matter system, the DM is treated as a halo surrounding the black hole [13, 14]. One widely used example is the Dehnen type halo model. Introduced by Walter Dehnen in 1993 to represent stellar bulges and DM halos, this model is defined by a three-parameter family of spherically symmetric density profiles, specified by the parameters (α, β, γ) [15]. Later on, it was developed in Refs. [16, 17]. Recently, within the Dehnen-type DM halo model, new Schwarzschild-like BH solutions embedded in a DM halo were derived for Dehnen-type density profiles (e.g., see [18–20]). Within the density profile of the Dehnen-type DM halo, recent investigations explore the impact of the DM halo on various astrophysical processes, including quasinormal modes, the BH shadow, and gravitational waveforms associated with periodic orbits [21–23].

High-frequency quasiperiodic oscillations (HF QPOs) in the X-ray flux coming from binary systems (e.g., BH and neutron star) provide a sensitive tool for probing the strong gravity region close to compact objects. QPOs

* xamidovtursunali@gmail.com

† sanjar@astrin.uz

‡ wuq@zjut.edu.cn

§ zhut05@zjut.edu.cn

appear as narrow peaks in the X-ray power-density spectrum. They originate in the inner accretion disks of compact objects such as black holes and neutron stars, and their frequencies depend only the curvature of the spacetime. Therefore, HF QPO measurements have been widely used to test alternative gravity models by analyzing X-ray data from accretion disks [24–28]. HF QPOs commonly appear as a pair of peaks whose upper ν_U and lower ν_L frequencies maintain an approximate 3 : 2 ratio. Such twin peak HF QPOs have been observed in multiple Galactic microquasars (e.g., GRO J1655-40, GRS 1915+105, XTE J1859+226, and XTE J1550-564) [29–31]. Many models interpret these QPO peaks as signatures of relativistic epicyclic motion or disk-oscillation resonances near the innermost stable circular orbit (ISCO) [32–34]. Despite ongoing debate over the precise mechanism behind their generation [35], a range of theories have been proposed, including models that incorporate magnetic fields around black holes [36–39]. Recent studies continue to evaluate and refine these explanations, exploring various resonance conditions and alternative spacetime metrics (see, e.g., [40–57]).

In this work, we investigate the solution of the BH-Dehnen-type DM halo and explore its impact in both weak and strong field regimes and derive the corresponding constraints on the parameters r_s and ρ_s . First, we study the motion of particles based on the principles of general relativity and derive the weak-field limit by matching the model to observational data from Mercury and the orbit of the S2 star. To constrain the model parameters r_s and ρ_s in strong gravitational fields, we turn to quasiperiodic oscillations. Because QPO frequencies depend only on the space-time curvature around black holes, they provide a powerful probe of general relativity and of possible dark-matter halo effects in the strong-field regime. Accordingly, we use QPO data from the microquasars GRO J1655-40, GRS 1915+105, XTE J1859+226, and XTE J1550-564 to set strong field limits on the parameters r_s and ρ_s .

The paper is structured as follows. In Sec. II, we introduce the spacetime metric describing a Schwarzschild black hole embedded in a dark matter halo and analyze particle dynamics. We also define the weak-field parameter space for the DM parameters r_s and ρ_s by examining the perihelion precession of Mercury and the orbit of the S2 star. In Sec. III, we explore the dynamics of epicyclic motion and derive general expressions for the upper and lower frequencies, while assessing how variations in the DM halo parameters influence these frequencies. In Sec. IV, we employ a Markov Chain Monte Carlo (MCMC) method to place strong-field constraints on r_s and ρ_s using observational data from four QPO sources. The paper concludes with a summary in Sec. V. We use geometric units $G = c = 1$ throughout this work.

II. THE SPACETIME METRIC AND THE DYNAMICS OF MOTION

The spacetime metric of the Schwarzschild BH in the Dehnen-(1, 4, 5/2) DM halo can be written as (see details in Ref. [19])

$$ds^2 = -f(r)dt^2 + f(r)^{-1}dr^2 + r^2(d\theta^2 + \sin^2\theta d\phi^2), \quad (1)$$

with

$$f(r) = 1 - \frac{2M}{r} - 32\pi\rho_s r_s^3 \sqrt{\frac{r+r_s}{r_s^2 r}}, \quad (2)$$

where r_s and ρ_s refer to the central halo density and radius, respectively.

Suppose that a neutral particle is moving around a Schwarzschild black hole embedded in a Dehnen-type dark matter halo. Then the Hamiltonian describing the massive particles motion can be written as follows [58]:

$$H = \frac{1}{2}g^{\mu\nu}p_\mu p_\nu = -\frac{m^2}{2}, \quad (3)$$

where p^μ denotes the fourmomentum of the neutral particle. The indices μ and ν run over (t, r, θ, ϕ) in the spherical coordinates. One can write the four-momentum as $p^\mu = m u^\mu$, where m is the particles rest mass and $u^\mu = dx^\mu/d\tau$ is its four-velocity, with τ denoting proper time. Since the metric in equation (1) does not depend explicitly on t or ϕ , one immediately obtains the following conserved quantities:

$$\frac{p_t}{m} = g_{tt}u^t = g_{tt}\frac{dt}{d\tau} = -\mathcal{E}, \quad (4)$$

$$\frac{p_\phi}{m} = g_{\phi\phi}u^\phi = g_{\phi\phi}\frac{d\phi}{d\tau} = \mathcal{L}, \quad (5)$$

where \mathcal{E} and \mathcal{L} are the specific energy and the specific angular momentum of the particle.

Using Eqs. (3–5), we can write the following equation:

$$\frac{1}{2}(g^{rr}p_r^2 + g^{\theta\theta}p_\theta^2) = -m^2 H_{pot}, \quad (6)$$

where

$$H_{pot} = \frac{1}{2}(g^{tt}\mathcal{E}^2 + g^{\phi\phi}\mathcal{L}^2 + 1). \quad (7)$$

Together with the relation $p_\mu = g_{\mu\nu}p^\nu$, we rewrite Eq. (6) as

$$g_{rr}\dot{r}^2 + g_{\theta\theta}\dot{\theta}^2 = -2H_{pot}, \quad (8)$$

where the over-dot denotes differentiation with respect to the proper time τ .

Assuming the particle moves in the equatorial plane ($\theta = \pi/2 = \text{const}$), so that $\dot{\theta} = 0$, the second term in Eq. (8) vanishes and the equation reduces to

$$g_{rr}\dot{r}^2 = -2H_{pot}. \quad (9)$$

Combining Eq. (5) with Eq. (9) gives the trajectory equation

$$\left(\frac{dr}{d\phi}\right)^2 = -\frac{2g_{\phi\phi}^2 H_{pot}}{g_{rr}\mathcal{L}^2}. \quad (10)$$

One can rewrite Eq. (10) in the following form using Eq. (7):

$$\left(\frac{dr}{d\phi}\right)^2 = \frac{r^4}{\mathcal{L}^2} \left[\mathcal{E}^2 - f(r) \left(1 + \frac{\mathcal{L}^2}{r^2} \right) \right]. \quad (11)$$

For a circular orbit ($r = \text{const}$) and hence $\dot{r} = 0$, Eq. (8) reduces to

$$g_{\theta\theta}\dot{\theta}^2 = -2H_{pot}. \quad (12)$$

For a particle on a circular orbit of radius R in the equatorial plane ($\theta = \pi/2$), the following conditions hold:

$$\begin{aligned} H_{pot}(R, \frac{\pi}{2}) &= 0, \\ \partial_r H_{pot}(r, \theta)|_{r=R} &= 0, \\ \partial_\theta H_{pot}(r, \theta)|_{\theta=\frac{\pi}{2}} &= 0. \end{aligned} \quad (13)$$

From Eqs. (4) and (5), one can determine the following expression for the angular velocity of the particle as measured by a distant observer:

$$\frac{d\phi}{dt} = \Omega = -\frac{g_{tt}}{g_{\phi\phi}} \cdot \frac{\mathcal{L}}{\mathcal{E}}. \quad (14)$$

On the other hand, as shown in Refs. [52, 59], the angular velocity can also be expressed as:

$$\Omega = \pm \sqrt{-\frac{g_{tt,r}}{g_{\phi\phi,r}}}. \quad (15)$$

Ω can be easily determined from the metric given in Eq. (1) using the above expression.

$$\Omega = \pm \sqrt{\left(\frac{M}{r^3} + \frac{8\pi\rho_s r_s^3}{r^3} \sqrt{\frac{r}{r+r_s}} \right) \csc^2(\theta)}. \quad (16)$$

By solving Eq. (7) under the condition given in Eq. (13) and considering the equality in Eq. (14), we obtain the following expressions for the energy and angular momentum:

$$\mathcal{E} = -\frac{g_{tt}}{\sqrt{-g_{tt} - g_{\phi\phi}\Omega^2}}, \quad (17)$$

$$\mathcal{L} = \frac{g_{\phi\phi}\Omega}{\sqrt{-g_{tt} - g_{\phi\phi}\Omega^2}}, \quad (18)$$

Using Eqs.(17) and (4), we can write the following expression for u^t

$$u^t = \frac{1}{\sqrt{-g_{tt} - g_{\phi\phi}\Omega^2}}, \quad (19)$$

The expressions for u^t , \mathcal{E} , and \mathcal{L} can be obtained using the metric in Eq. (1) and the angular velocity defined in Eq. (16)

$$u^t = \left(1 - \frac{3M}{r} - \frac{8\pi\rho_s r_s^2 (4r + 5r_s)}{\sqrt{r(r+r_s)}} \right)^{-\frac{1}{2}}, \quad (20)$$

$$\mathcal{E} = \left(1 - \frac{2M}{r} - 32\pi\rho_s r_s^3 \sqrt{\frac{r+r_s}{r_s^2 r}} \right) \times u^t, \quad (21)$$

$$\mathcal{L} = \sqrt{r \left(M + 8\pi\rho_s r_s^3 \sqrt{\frac{r}{r+r_s}} \right) \sin^2(\theta)} \times u^t. \quad (22)$$

Let us perform the following transformation:

$$\xi = \frac{1}{r}, \quad \frac{d\xi}{d\phi} = -\frac{1}{r^2} \frac{dr}{d\phi}. \quad (23)$$

As a result, Eq. (11) takes the form

$$\left(\frac{d\xi}{d\phi} \right)^2 = \frac{\mathcal{E}^2}{\mathcal{L}^2} - \frac{f(\xi)}{\mathcal{L}^2} (1 + \mathcal{L}^2 \xi^2), \quad (24)$$

where the function $f(\xi)$ is given by

$$f(\xi) = 1 - 2M\xi - 32\pi\rho_s r_s^3 \sqrt{\frac{1+r_s\xi}{r_s^2}}. \quad (25)$$

Differentiating Eq. (24) with respect to ϕ yields the geodesic equation for a massive test particle.

$$\frac{d^2\xi}{d\phi^2} = \frac{M}{\mathcal{L}^2} - \xi + \frac{g(\xi)}{\mathcal{L}^2}, \quad (26)$$

where

$$\frac{g(\xi)}{\mathcal{L}^2} = 3M\xi^2 + \frac{8\pi\rho_s r_s^2}{\sqrt{1+r_s\xi}} \left(\frac{r_s}{\mathcal{L}^2} + 4\xi + 5r_s\xi^2 \right). \quad (27)$$

Following the approach outlined in Ref. [60], the perihelion shift after a complete revolution is defined as:

$$\Delta\phi = \frac{\pi}{\mathcal{L}^2} \left| \frac{dg(\xi)}{d\xi} \right|_{\xi=\frac{1}{b}}. \quad (28)$$

Using Eq. (27), we can determine the perihelion shift as follows

$$\begin{aligned} \Delta\phi &= \frac{6\pi M}{\mathcal{R}} + 4\pi^2 \rho_s r_s^2 \sqrt{\frac{\mathcal{R}+r_s}{\mathcal{R}}} \cdot \frac{8\mathcal{R}^2 + 24\mathcal{R}r_s + 15r_s^2}{(\mathcal{R}+r_s)^2} \\ &\quad - \frac{4\pi^2 \rho_s r_s^4}{\mathcal{L}^2} \left(\frac{\mathcal{R}}{\mathcal{R}+r_s} \right)^{3/2}, \end{aligned} \quad (29)$$

where we have defined $\mathcal{R} = a(1-e^2)$ with a and e representing the semi-major axis and eccentricity of the orbit, respectively.

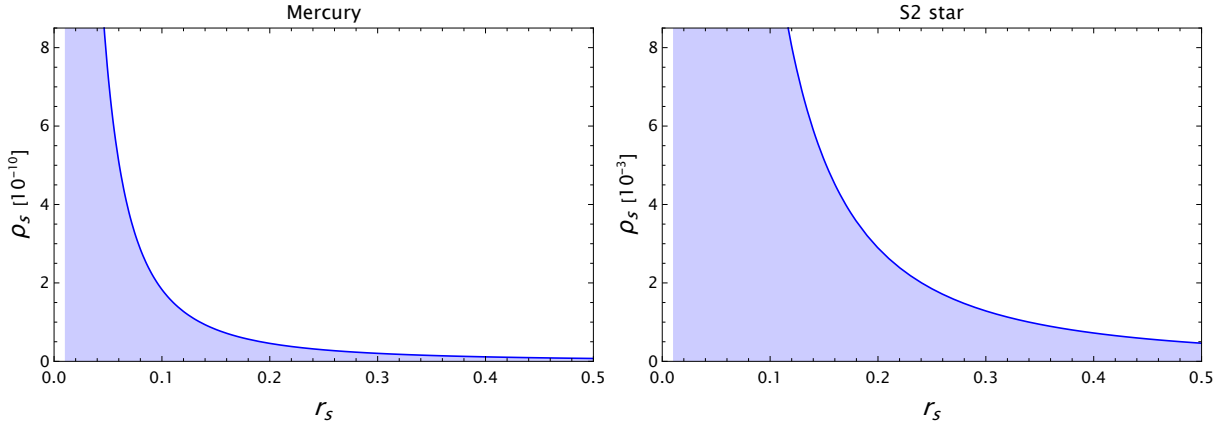


FIG. 1. Parameter space between the dimensionless halo radius r_s and the dimensionless dark matter density ρ_s . The shaded region indicates the observationally allowed values of (r_s, ρ_s) from Mercury (left) and S2 star (right) measurements.

To recover physical dimensions, the mass M , the angular momentum L^2 , the dark matter halo density ρ_s , and the halo radius r_s are rescaled as

$$M \Rightarrow GM/c^2, \quad (30)$$

$$L^2 \Rightarrow GMa(1-e^2)/c^2, \quad (31)$$

$$\rho_s \Rightarrow \frac{3c^4}{32\pi G^2 M^2} \rho_s, \quad (32)$$

$$r_s \Rightarrow \frac{GM}{c^2} r_s. \quad (33)$$

The dark matter halo density ρ_s and the halo radius r_s on the right-hand side are therefore *dimensionless*: they give the numerical values of the corresponding physical quantities when expressed in the units $3c^4/(32\pi G^2 M^2)$ and GM/c^2 , respectively.

With these conventions, the perihelion shift after one full revolution, Eq. (29), becomes

$$\Delta\phi = 6\pi\alpha + 3\pi\rho_s r_s^2 \sqrt{1+\alpha r_s} \left(1 + \frac{\alpha r_s}{1+\alpha r_s} - \frac{\alpha r_s^2}{8(1+\alpha r_s)} - \frac{\alpha^2 r_s^2}{8(1+\alpha r_s)^2} + \frac{\alpha^2 r_s^3}{8(1+\alpha r_s)^2} \right), \quad (34)$$

where

$$\alpha = \frac{GM}{ac^2(1-e^2)}. \quad (35)$$

Here, ρ_s and r_s denote the dimensionless dark matter halo density and the halo radius, respectively.

We use observational data from the perihelion shifts of Mercury and the S2 star to determine constraints on r_s and ρ_s . Below, we present the observational data for the orbital parameters and the perihelion shift of Mercury and the S2 star [51, 61–64].

Mercury:

$$\frac{2GM_\odot}{c^2} = 2.95325008 \times 10^3 [\text{m}],$$

$$a = 5.7909175 \times 10^{10} [\text{m}],$$

$$e = 0.20563069,$$

$$\Delta\phi_{\text{obs}} = 2\pi \times (7.98734 \pm 0.00037) \times 10^{-8} \text{ rad/rev.}$$

S2 star:

$$M_{\text{Sgr A}^*} = 4.260 \times 10^6 M_\odot,$$

$$a_{\text{S2}} = 970 [\text{au}],$$

$$1 \text{ au} = 1.495978707 \times 10^{11} [\text{m}],$$

$$e_{\text{S2}} = 0.884649,$$

$$T_{\text{S2}} = 16.052 [\text{years}],$$

$$\Delta\phi_{\text{obs}} = 48.298 f_{\text{SP}} \left[''/\text{year} \right], f_{\text{SP}} = 1.10 \pm 0.19.$$

Based on these data, we use Eq. (34) to plot the parameter space of r_s and ρ_s for both Mercury and the S2 star (see Fig. 1). From Fig. 1, it is evident that the parameter space for the S2 star is larger than that for Mercury. This indicates that the influence of the DM halo becomes more evident near more massive objects. It is evident that the scale of ρ_s is of the order of about 10^{-10} in the weak field and its ratio accordingly refers to the order of 10^{-7} between the solar system and the supermassive BH at the center of the Sgr A* galaxy, similar to the ratio $M_\odot/M_{\text{Sgr A}^*}$. This highlights that the effects of the DM halo become observable only around supermassive BHs.

III. THE DYNAMICS OF EPICYCLIC MOTION

Consider a particle moving along a stable circular orbit of radius $r = R$ in the equatorial plane $\theta = \pi/2$. A slight deviation of a test particle from its stable circular orbit leads to oscillations around the equilibrium radius,

known as epicyclic motion, which is characterized by the epicyclic frequencies. The deviations in r and θ due to small perturbations can be written as:

$$r = R + \delta r \quad \text{and} \quad \theta = \pi/2 + \delta\theta. \quad (36)$$

A Taylor series expansion of H_{pot} about $r = R$ and $\theta = \pi/2$ allows us to determine the effect of the perturbation.

$$\begin{aligned} H_{pot}(r, \theta) &= H_{pot}(R, \frac{\pi}{2}) + \delta r \partial_r H_{pot}(r, \theta) \Big|_{R, \frac{\pi}{2}} + \\ &+ \delta\theta \partial_\theta H_{pot}(r, \theta) \Big|_{R, \frac{\pi}{2}} + \delta r \delta\theta \partial_r \partial_\theta H_{pot}(r, \theta) \Big|_{R, \frac{\pi}{2}} + \\ &+ \frac{1}{2} \delta r^2 \partial_r^2 H_{pot}(r, \theta) \Big|_{R, \frac{\pi}{2}} + \frac{1}{2} \delta\theta^2 \partial_\theta^2 H_{pot}(r, \theta) \Big|_{R, \frac{\pi}{2}} + \\ &+ \mathcal{O}(\delta r^3, \delta\theta^3). \end{aligned} \quad (37)$$

Applying Eq. (13) and neglecting higher-order terms $\mathcal{O}(\delta r^3, \delta\theta^3)$ yields the following expression:

$$H_{pot}(r, \theta) = \frac{1}{2} \delta r^2 \partial_r^2 H_{pot}(r, \theta) \Big|_{R, \frac{\pi}{2}} + \frac{1}{2} \delta\theta^2 \partial_\theta^2 H_{pot}(r, \theta) \Big|_{R, \frac{\pi}{2}}. \quad (38)$$

Using Eq. (36) in Eq. (8) and incorporating Eq. (38), we arrive at the following expression:

$$\begin{aligned} g_{rr} \delta \ddot{r} + g_{\theta\theta} \delta \dot{\theta}^2 &= -\delta r^2 \partial_r^2 H_{pot}(r, \theta) \Big|_{R, \frac{\pi}{2}} - \\ &- \delta\theta^2 \partial_\theta^2 H_{pot}(r, \theta) \Big|_{R, \frac{\pi}{2}}. \end{aligned} \quad (39)$$

Differentiating both sides of the above equation with respect to proper time τ yields:

$$\begin{aligned} \delta \dot{r} \left[g_{rr} \delta \ddot{r} + \partial_r^2 H_{pot}(r, \theta) \Big|_{R, \frac{\pi}{2}} \delta r \right] + \\ + \delta \dot{\theta} \left[g_{rr} \delta \ddot{\theta} + \partial_\theta^2 H_{pot}(r, \theta) \Big|_{R, \frac{\pi}{2}} \delta \theta \right] = 0. \end{aligned} \quad (40)$$

Since the solutions $\delta \dot{r} = 0$ and $\delta \dot{\theta} = 0$ correspond to no oscillation, they are not physically relevant. A valid solution can be obtained only when the terms within the brackets vanish [38]

$$\delta \ddot{r} + \Omega_r^2 \delta r = 0 \quad \text{and} \quad \delta \ddot{\theta} + \Omega_\theta^2 \delta \theta = 0, \quad (41)$$

where

$$\Omega_r^2 = \frac{\partial_r^2 H_{pot}(r, \theta)|_{r_c, \frac{\pi}{2}}}{g_{rr}}, \quad (42)$$

$$\Omega_\theta^2 = \frac{\partial_\theta^2 H_{pot}(r, \theta)|_{r_c, \frac{\pi}{2}}}{g_{\theta\theta}}. \quad (43)$$

Here, Ω_r and Ω_θ denote the local epicyclic frequencies. However, since many astronomical sources are located at large distances, the epicyclic frequencies as measured by a distant observer are of greater physical relevance

than the local ones. The relation between the local and distant epicyclic frequencies is expressed by the following equation:

$$\omega_{\text{distant}} = \frac{\Omega_{\text{local}}}{u^t}, \quad (44)$$

Thus, the epicyclic frequencies as measured by a distant observer are given by the following expressions:

$$\begin{aligned} \omega_r^2 &= \frac{M}{r^3} - \frac{6M^2}{r^4} - \frac{8\pi\rho_s r_s^2 (4r^2 + 18rr_s + 15r_s^2) M}{r^5 \left(\frac{r+r_s}{r} \right)^{3/2}} \\ &+ \frac{4\pi\rho_s r_s^3 \left(-160\pi\rho_s r_s^3 - 64\pi r \rho_s r_s^2 + \frac{2r+3r_s}{\sqrt{\frac{r+r_s}{r}}} \right)}{r^3 (r+r_s)}, \end{aligned} \quad (45)$$

$$\omega_\theta^2 = \frac{M}{r^3} + \frac{8\pi\rho_s r_s^3}{r^3} \sqrt{\frac{r}{r+r_s}}. \quad (46)$$

To convert the frequency to SI units (Hz), the following transformation is applied:

$$\nu_i = \frac{\omega_i}{2\pi} \frac{c^3}{GM}. \quad (47)$$

Fig. 2 shows the epicyclic frequencies ν_r and ν_θ as functions of r/M , as measured by a distant observer, for various values of the dark matter halo density ρ_s and halo radius r_s . From the plots, it is evident that both ρ_s and r_s influence the epicyclic frequencies in a similar manner. Specifically, as ρ_s and r_s increase, the θ -component of the epicyclic frequency, ν_θ , increases, while the radial component, ν_r , decreases and shifts to larger radii.

This behavior can be interpreted as the result of an enhanced gravitational pull caused by the increase in ρ_s and r_s , effectively mimicking the presence of additional mass at the center of the black hole. In other words, the gravitational field becomes stronger. Thus, the rise in ν_θ results from the growth of the second term in Eq. (46). Additionally, the stronger gravitational field pushes the innermost stable circular orbit (ISCO) outward, causing radial oscillations to occur at larger radii. As a result, the radial epicyclic frequency ν_r shifts to the right and decreases in magnitude.

IV. CONSTRAINTS ON THE PARAMETERS OF THE DARK MATTER HALO THROUGH THE ASTROPHYSICAL QUASIPERIODIC OSCILLATIONS

In this section, we constrain the dark matter halo density ρ_s and halo radius r_s using MCMC analysis based on observational data from four QPO sources. The validated observational data for these sources are listed in Table I. We employ the forced resonance model to describe the upper and lower frequencies, which are expressed in this model as [51, 65, 66]:

$$\nu_{up} = \nu_\theta + \nu_r, \quad \nu_{low} = \nu_\theta. \quad (48)$$

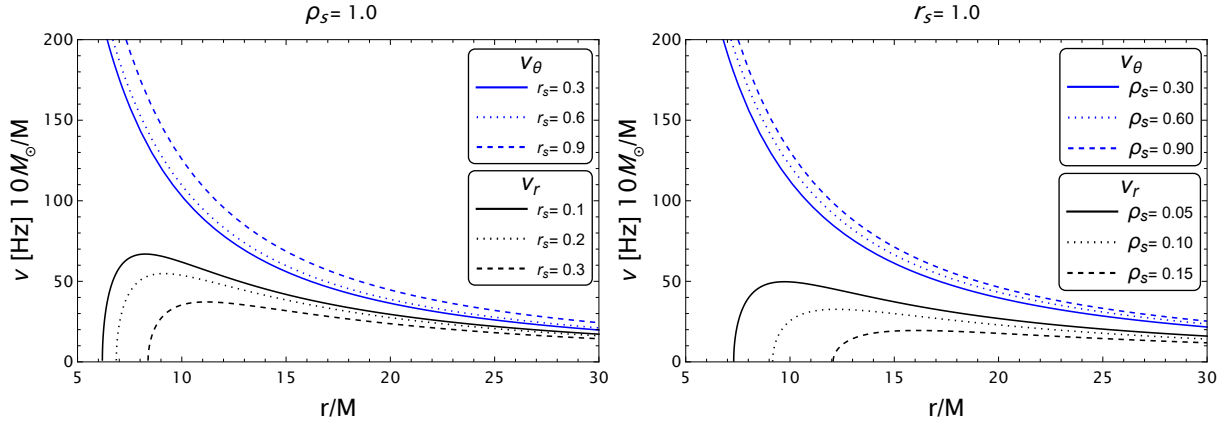


FIG. 2. The radial profile of the frequencies ν_θ and ν_r measured by a distant observer is shown as a function of r/M for different values of ρ_s and r_s .

	GRS 1915 + 105 [68]	XTE J1859+226 [69, 70]	XTE J1550 - 564 [71, 72]	GRO J1655 - 40 [73]
$M[M_\odot]$	$12.4^{+2.0}_{-1.8}$	$7.85^{+0.46}_{-0.46}$	$9.1^{+0.61}_{-0.61}$	$5.4^{+0.3}_{-0.3}$
$\nu_U [\text{Hz}]$	$168^{+3.0}_{-3.0}$	$227.5^{+2.1}_{-2.4}$	$276^{+3.0}_{-3.0}$	$441^{+2.0}_{-2.0}$
$\nu_L [\text{Hz}]$	$113^{+5.0}_{-5.0}$	$128.6^{+1.6}_{-1.8}$	$184^{+5.0}_{-5.0}$	$298^{+4.0}_{-4.0}$

TABLE I. Masses and corresponding the upper and the lower QPO frequencies for the X-ray binaries analyzed in this work.

We use the Python package the *emcee*, which implements Markov Chain Monte Carlo (MCMC) sampling, to find the best-fit values of the dark matter halo density ρ_s and scale radius r_s [67]. Bayes' theorem yields the posterior probability distribution

$$P(\Theta | D, \mathcal{M}) = \frac{\mathcal{L}(D | \Theta, \mathcal{M}) \pi(\Theta | \mathcal{M})}{P(D | \mathcal{M})},$$

where $P(\Theta | D, \mathcal{M})$ is the *posterior*, $\mathcal{L}(D | \Theta, \mathcal{M})$ is the *likelihood*, $\pi(\Theta | \mathcal{M})$ is the *prior*, and $P(D | \mathcal{M})$ is a *normalization constant*.

We assign a Gaussian prior to the mass of the black hole M ,

$$\pi(M) = \frac{1}{\sqrt{2\pi}\sigma} \exp\left[-\frac{(M - M_0)^2}{2\sigma^2}\right], \quad (49)$$

$M_{\min} < M < M_{\max}$, and $\pi(M) = 0$ outside that interval.

For the remaining parameters $\theta_i = [r, \rho_s, r_s]$ we use independent uniform (tophat) priors,

$$\pi(\theta_i) = \begin{cases} (\theta_{i,\max} - \theta_{i,\min})^{-1}, & \theta_{i,\min} < \theta_i < \theta_{i,\max}, \\ 0, & \text{otherwise.} \end{cases}$$

The numerical limits $\theta_{i,\min}$ and $\theta_{i,\max}$ are given in Table II.

Assuming independence, the full prior factorises as

$$\pi(\Theta) = \pi(M) \pi(r) \pi(\rho_s) \pi(r_s),$$

where $\Theta = (M, r, \rho_s, r_s)$.

Parameters	GRS 1915 + 105		XTE J1859+226		XTE J1550 - 564		GRO J1655 - 40	
	μ	σ	μ	σ	μ	σ	μ	σ
M/M_\odot	12.4	0.6	7.85	0.03	9.1	0.005	5.2	0.03
r/M	Uniform (6, 15)							
ρ_s/M^2	Uniform [0, 0.6]	Uniform [0, 0.4]						
r_s/M	Uniform [0, 0.6]	Uniform [0, 0.4]						

TABLE II. Prior distributions used in the MCMC analysis: Gaussian priors for the masses (μ mean, σ standard deviation) and uniform priors for the orbital radius r/M as well as for the dark matter halo density ρ_s/M^2 and halo radius r_s/M - for each X-ray binary.

Using the upper frequency ν_{up} and lower frequency ν_{low} formulas in Eqs. (48), we construct a joint Gaussian likelihood that simultaneously incorporates the observational ν_{up} and ν_{low} data listed in Table I. The total log-likelihood is

$$\ln \mathcal{L} = \ln \mathcal{L}_U + \ln \mathcal{L}_L, \quad (50)$$

where the contribution from the upper (U) frequencies is

$$\ln \mathcal{L}_U = -\frac{1}{2} \sum_i \frac{(\nu_{U,\text{obs}}^i - \nu_{U,\text{mod}}^i)^2}{(\sigma_{U,\text{obs}}^i)^2}, \quad (51)$$

and the term for the lower (L) frequencies is

$$\ln \mathcal{L}_L = -\frac{1}{2} \sum_i \frac{(\nu_{L,\text{obs}}^i - \nu_{L,\text{mod}}^i)^2}{(\sigma_{L,\text{obs}}^i)^2}. \quad (52)$$

Here, $\nu_{U,\text{obs}}^i$ and $\nu_{L,\text{obs}}^i$ are the measured upper and lower QPO frequencies, $\nu_{U,\text{mod}}^i$ and $\nu_{L,\text{mod}}^i$ are the corresponding model predictions, and $\sigma_{U,\text{obs}}^i$ and $\sigma_{L,\text{obs}}^i$ denote the corresponding statistical uncertainties for the associated quantities.

With this likelihood we explore the four-parameter space $[r, M, \rho_s, r_s]$ via MCMC. The median (best-fit) val-

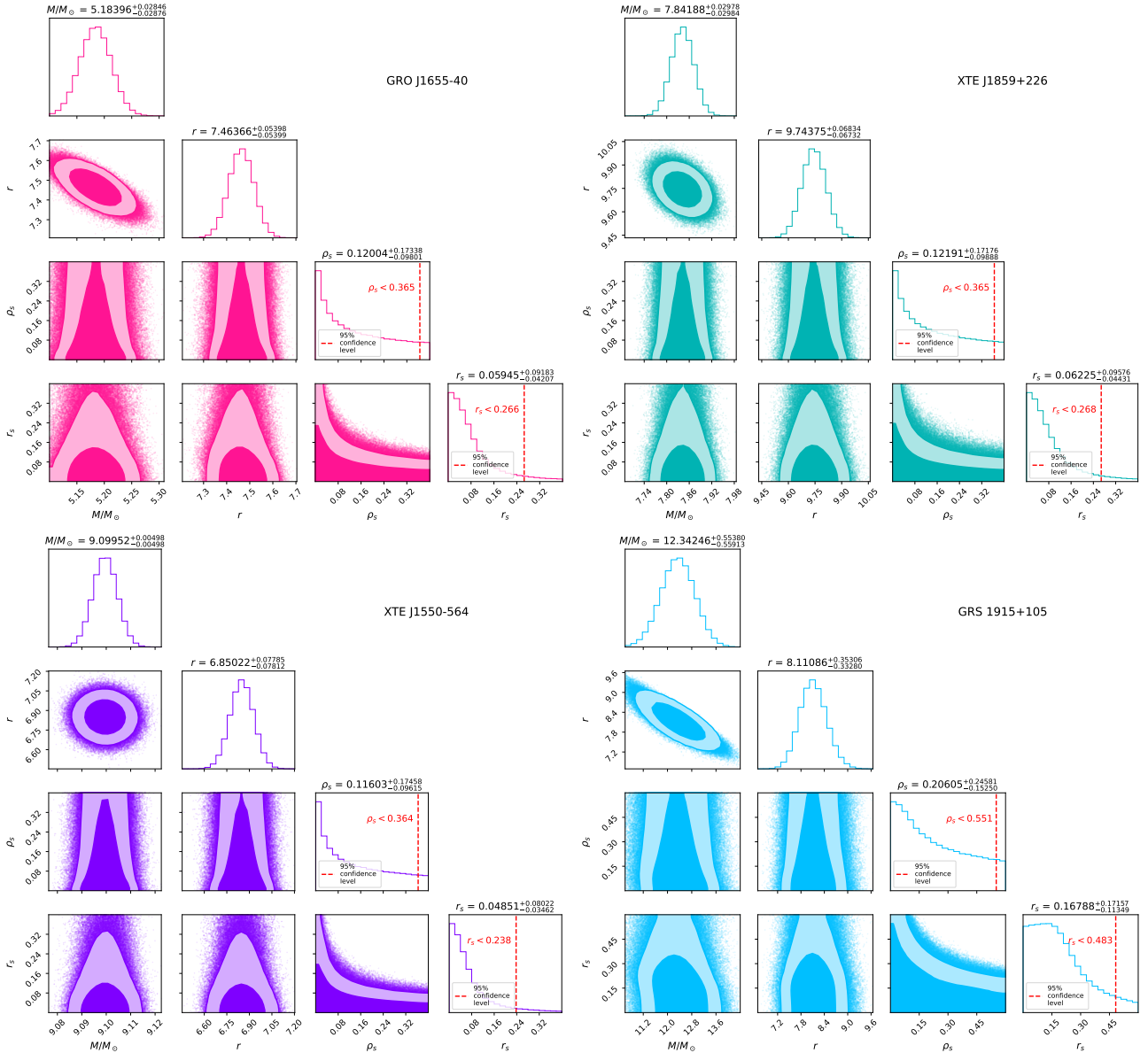


FIG. 3. Posterior probability distributions for the black hole mass (M), the dimensionless QPO radius (r/M), and the dark matter halo density (ρ_s) and halo radius (r_s) - obtained with the forced-resonance model. Vertical red dashed lines mark the 95 % credible upper limits on ρ_s and r_s .

ues are reported in Table III, while Fig. 3 shows the posterior probability density distributions for four X-ray binaries. The shaded regions in Fig. 3 mark the 68 %, and 95 % confidence level, illustrating the statistical uncertainties of the inferred dark matter halo parameters ρ_s and r_s .

Fig. 4 compares the model predictions - obtained from the best-fit MCMC parameters - with the observed twin-QPO frequencies. The agreement is excellent for GRS 1915+105 and remains good for GRO J1655-40. By contrast, the model does not match the observations for XTE J1550-564 and XTE J1859+226.

Parameters	GRS 1915 + 105	XTE J1859+226	XTE J1550 - 564	GRO J1655 - 40
M/M_\odot	$12.342^{+0.554}_{-0.559}$	$9.099^{+0.005}_{-0.005}$	$7.842^{+0.030}_{-0.030}$	$5.184^{+0.028}_{-0.029}$
r/M	$8.111^{+0.353}_{-0.333}$	$9.744^{+0.068}_{-0.067}$	$6.850^{+0.078}_{-0.078}$	$7.464^{+0.054}_{-0.054}$
ρ_s/M^2	< 0.551	< 0.365	< 0.364	< 0.365
r_s/M	< 0.483	< 0.268	< 0.238	< 0.266

TABLE III. Best-fit black-hole masses (M) and dimensionless QPO radii (r/M), together with upper limits on the dark matter halo density (ρ_s/M^2) and halo radius (r_s/M).

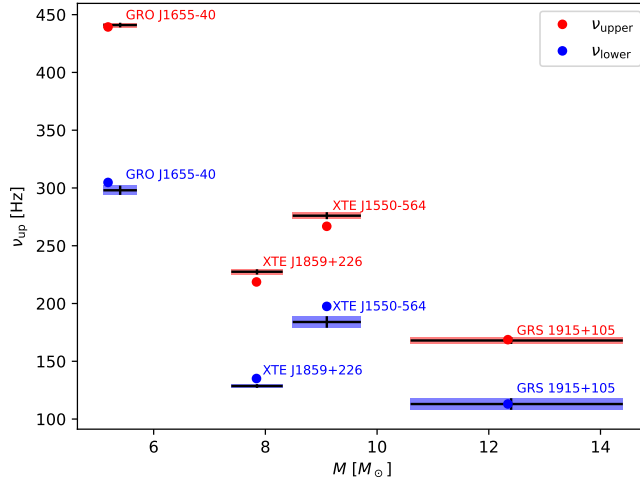


FIG. 4. Comparison between model predictions and observational data for HF QPOs in X-ray binary systems. Red and blue dots represent the model frequencies (upper and lower, respectively) calculated using best-fit parameters obtained from MCMC analysis. The red and blue error boxes show the corresponding observational data, including uncertainties in both mass and QPO frequency. Red indicates the upper frequency (ν_{upper}), while blue represents the lower frequency (ν_{lower}). Each source is labeled accordingly.

V. CONCLUSIONS

In this work, we examined a Schwarzschild BH embedded in a Dehnen-type (1, 4, 5/2) DM halo. By combining theory with observational constraints, we showed that the DM halo can alter the orbits of objects measurably. A perihelion shift expression, applied to Mercury and the orbit of the S2 star, reveals that the admissible (ρ_s, r_s) parameter space broadens with increasing mass of the BH, implying that DM halo effects are more evident around more massive orbits. Our findings show that the effects of the DM halo become observable only around supermassive BHs.

Our analysis of QPOs shows that epicyclic frequencies can carry a clear halo signature and indicates that increasing either the halo radius r_s or density ρ_s raises the vertical (latitudinal) epicyclic frequency ν_θ , while it lowers the radial frequency ν_r . This behavior explained by the extra gravitational pull of the DM halo, which shifts the innermost stable circular orbit (r_{ISCO}) to larger radii.

Twin-QPO measurements place empirical limits on the halo. To constrain the halo parameters empirically, we perform MCMC analysis with the *emcee* sampler [67]. Figure 3 presents the posterior distributions for four Galactic microquasars, including GRO J1655-40, GRS 1915+105, XTE J1859+226, and XTE J1550-564. The corresponding best-fit and upper limit values are listed in Table III. Using these data, we compute model QPO frequencies and compare them with the observed values,

as shown in Fig. 4. The match is in good agreement with GRS 1915+105 and remains satisfactory for GRO J1655-40, whereas discrepancies persist for XTE J1550-564 and XTE J1859-226.

Our combined geodesic analysis and constraints using the data of QPOs demonstrate that timelike orbits and epicyclic oscillations around a BH can serve as sensitive probes of the surrounding DM halo.

It must be emphasized that the analyses conducted on the time-like geodesics of particles and the QPOs generated by particles' epicyclic motion around the BH surrounded by a Dehnen-type DM halo and the constraints on the DM halo parameters by adapting the observed frequencies of these mentioned microquasars are of significant astrophysical importance. The results improve our understanding of dark matter and enable us to discriminate the Dehnen-type DM halo from alternative halo profiles, which could be crucial for identifying DM signatures in future analysis and astronomical observations.

ACKNOWLEDGMENTS

S.S. is supported by the National Natural Science Foundation of China under Grant No. W2433018. T. Zhu is also supported by the National Natural Science Foundation of China under Grants No. 12275238, the National Key Research and Development Program of China under Grant No. 2020YFC2201503, and the Zhejiang Provincial Natural Science Foundation of China under Grants No. LR21A050001 and No. LY20A050002.

[1] K. Akiyama and et al. (Event Horizon Telescope Collaboration), *Astrophys. J.* **875**, L1 (2019), arXiv:1906.11238

[astro-ph.GA].

- [2] K. Akiyama and et al. (Event Horizon Telescope Collaboration), *Astrophys. J.* **875**, L6 (2019), arXiv:1906.11243 [astro-ph.GA].
- [3] B. P. Abbott and et al. (Virgo and LIGO Scientific Collaborations), *Phys. Rev. Lett.* **116**, 061102 (2016), arXiv:1602.03837 [gr-qc].
- [4] B. P. Abbott and et al. (Virgo and LIGO Scientific Collaborations), *Phys. Rev. Lett.* **116**, 241102 (2016), arXiv:1602.03840 [gr-qc].
- [5] Planck Collaboration and Aghanim, *Astron. Astrophys.* **641**, A6 (2020), arXiv:1807.06209 [astro-ph.CO].
- [6] V. C. Rubin and W. K. Ford, Jr., *Astrophys. J.* **159**, 379 (1970).
- [7] M. Karamazov, L. Timko, and D. Heyrovsk, *Astrophys. J.* **922**, 72 (2021).
- [8] Q. Qi, Y. Meng, X.-J. Wang, and X.-M. Kuang, *Eur. Phys. J. C* **83**, 1043 (2023).
- [9] C. Bhm and P. Fayet, *Nucl. Phys. B* **683**, 219 (2004).
- [10] G. Bertone, D. Hooper, and J. Silk, *Phys. Rep.* **405**, 279 (2005).
- [11] J. L. Feng, M. Kaplinghat, H. Tu, and H.-B. Yu, *J. Cosmol. Astropart. Phys.* **2009**, 004 (2009).
- [12] M. Schumann, *J. Phys. G* **46**, 103003 (2019).
- [13] P. Gondolo and J. Silk, *Phys. Rev. Lett.* **83**, 1719 (1999).
- [14] G. BERTONE and D. MERRITT, *Mod. Phys. Lett. A* **20**, 1021 (2005), <https://doi.org/10.1142/S0217732305017391>.
- [15] W. Dehnen, *Mon. Not. R. Astron. Soc.* **265**, 250 (1993).
- [16] T. Matos and D. Nunez, *Rev. Mex. Fis.* **51**, 71 (2005).
- [17] Z. Xu, X. Hou, X. Gong, and J. Wang, *J. Cosmol. Astropart. Phys.* **2018**, 038 (2018), arXiv:1803.00767 [gr-qc].
- [18] M. M. Gohain, P. Phukon, and K. Bhuyan, *Phys. Dark Univ.* **46**, 101683 (2024), arXiv:2407.02872 [gr-qc].
- [19] A. Al-Badawi, S. Shaymatov, and Y. Sekhmani, *J. Cosmol. Astropart. Phys.* **2025**, 014 (2025), arXiv:2411.01145 [gr-qc].
- [20] U. Uktamov, S. Shaymatov, and B. Ahmedov, *arXiv e-prints*, arXiv:2505.20031 (2025), arXiv:2505.20031 [gr-qc].
- [21] A. Al-Badawi and S. Shaymatov, *Chin. Phys. C* **49**, 055101 (2025), arXiv:2501.15397 [gr-qc].
- [22] A. Al-Badawi and S. Shaymatov, *Commun. Theor. Phys.* **77**, 035402 (2025).
- [23] M. Alloqulov, T. Xamidov, S. Shaymatov, and B. Ahmedov, *arXiv e-prints*, arXiv:2504.05236 (2025), arXiv:2504.05236 [gr-qc].
- [24] M. A. Abramowicz and P. C. Fragile, *Living Rev. Relativ.* **16**, 1 (2013), arXiv:1104.5499 [astro-ph.HE].
- [25] C. Bambi, *Phys. Rev. D* **85**, 043002 (2012), arXiv:1201.1638 [gr-qc].
- [26] C. Bambi, J. Jiang, and J. F. Steiner, *Class. Quantum Gravity* **33**, 064001 (2016), arXiv:1511.07587 [gr-qc].
- [27] A. Tripathi, J. Yan, Y. Yang, Y. Yan, M. Garnham, Y. Yao, S. Li, Z. Ding, A. B. Abdikamalov, D. Ayzenberg, C. Bambi, T. Dauser, J. A. Garcia, J. Jiang, and S. Nampalliwar, *arXiv e-prints* (2019), arXiv:1901.03064 [gr-qc].
- [28] T. Xamidov, U. Uktamov, S. Shaymatov, and B. Ahmedov, *Phys. Dark Universe* **47**, 101805 (2025).
- [29] W. Kluzniak and M. A. Abramowicz, *Acta Phys. Pol. B* **32**, 3605 (2001).
- [30] G. Török, M. A. Abramowicz, W. Klużniak, and Z. Stuchlík, *Astron. Astrophys.* **436**, 1 (2005).
- [31] R. A. Remillard, J. E. McClintock, J. A. Orosz, and A. M. Levine, *Astrophys. J.* **637**, 1002 (2006), arXiv:astro-ph/0407025 [astro-ph].
- [32] Z. Stuchlík, A. Kotrlová, and G. Török, *Astron. Astrophys.* **552**, A10 (2013), arXiv:1305.3552 [astro-ph.HE].
- [33] L. Stella, M. Vietri, and S. M. Morsink, *Astrophys. J.* **524**, L63 (1999), arXiv:astro-ph/9907346 [astro-ph].
- [34] L. Rezzolla, S. Yoshida, T. J. Maccarone, and O. Zanotti, *Mon. Not. R. Astron. Soc.* **344**, L37 (2003), arXiv:astro-ph/0307487.
- [35] G. Török, A. Kotrlová, E. Šrámková, and Z. Stuchlík, *Astron. Astrophys.* **531**, A59 (2011), arXiv:1103.2438 [astro-ph.HE].
- [36] A. Tursunov, Z. Stuchlík, M. Kološ, N. Dadhich, and B. Ahmedov, *Astrophys. J.* **895**, 14 (2020).
- [37] R. Pánis, M. Kološ, and Z. Stuchlík, *Eur. Phys. J. C* **79**, 479 (2019), arXiv:1905.01186 [gr-qc].
- [38] S. Shaymatov, J. Vrba, D. Malafarina, B. Ahmedov, and Z. Stuchlík, *Phys. Dark Universe* **30**, 100648 (2020), arXiv:2005.12410 [gr-qc].
- [39] S. Shaymatov, M. Jamil, K. Jusufi, and K. Bamba, *Eur. Phys. J. C* **82**, 636 (2022), arXiv:2205.00270 [gr-qc].
- [40] C. Germanà, *Phys. Rev. D* **98**, 083025 (2018), arXiv:1810.12426 [astro-ph.HE].
- [41] M. Tarnopolski and V. Marchenko, *Astrophys. J.* **911**, 20 (2021), arXiv:2102.05330 [astro-ph.HE].
- [42] V. I. Dokuchaev and Y. N. Eroshenko, *Phys. Usp.* **58**, 772 (2015), arXiv:1512.02943 [astro-ph.HE].
- [43] M. Kološ, Z. Stuchlík, and A. Tursunov, *Class. Quant. Grav.* **32**, 165009 (2015), arXiv:1506.06799 [gr-qc].
- [44] A. N. Aliev, G. D. Esmer, and P. Talazan, *Class. Quant. Grav.* **30**, 045010 (2013), arXiv:1205.2838 [gr-qc].
- [45] Z. Stuchlik, P. Slany, and G. Torok, *Astron. Astrophys.* **470**, 401 (2007), arXiv:0704.1252 [astro-ph].
- [46] L. Titarchuk and N. Shaposhnikov, *Astrophys. J.* **626**, 298 (2005), arXiv:astro-ph/0503081.
- [47] M. Azreg-Aïnou, Z. Chen, B. Deng, M. Jamil, T. Zhu, Q. Wu, and Y.-K. Lim, *Phys. Rev. D* **102**, 044028 (2020), arXiv:2004.02602 [gr-qc].
- [48] K. Jusufi, M. Azreg-Aïnou, M. Jamil, S.-W. Wei, Q. Wu, and A. Wang, *Phys. Rev. D* **103**, 024013 (2021), arXiv:2008.08450 [gr-qc].
- [49] M. Ghasemi-Nodehi, M. Azreg-Aïnou, K. Jusufi, and M. Jamil, *Phys. Rev. D* **102**, 104032 (2020), arXiv:2011.02276 [gr-qc].
- [50] J. Rayimbaev, B. Majeed, M. Jamil, K. Jusufi, and A. Wang, *Phys. Dark Universe* **35**, 100930 (2022), arXiv:2202.11509 [gr-qc].
- [51] S. Shaymatov, B. Ahmedov, M. De Laurentis, M. Jamil, Q. Wu, A. Wang, and M. Azreg-Aïnou, *Astrophys. J.* **959**, 6 (2023), arXiv:2307.10804 [gr-qc].
- [52] S. Shaymatov, K. Jusufi, M. Alloqulov, and B. Ahmedov, *Eur. Phys. J. Plus* **138**, 997 (2023), arXiv:2303.06494 [gr-qc].
- [53] G. Mustafa, G. D. Acan Yıldız, F. Javed, S. Maurya, E. Güdeklı, and F. Atamurotov, *Phys. Dark Universe* **46**, 101647 (2024), 10.1016/j.dark.2024.101647.
- [54] C. Liu, H. Siew, T. Zhu, Q. Wu, Y. Sun, Y. Zhao, and H. Xu, *JCAP* **11**, 096 (2023), arXiv:2305.12323 [gr-qc].
- [55] M.-Y. Guo, M.-H. Wu, X.-M. Kuang, and H. Guo, *Eur. Phys. J. C* **85**, 95 (2025).
- [56] C. Liu, H. Siew, T. Zhu, Q. Wu, Y. Zhao, and H. Xu, (2023), arXiv:2311.12423 [astro-ph.HE].

- [57] J.-M. Yan, C. Liu, T. Zhu, Q. Wu, and A. Wang, *Phys. Rev. D* **107** (2023), 10.1103/physrevd.107.084043.
- [58] C. W. Misner, K. S. Thorne, and J. A. Wheeler, *Gravitation* (W. H. Freeman, San Francisco, 1973).
- [59] S. Shaymatov, P. Sheoran, and S. Siwach, *Phys. Rev. D* **105**, 104059 (2022), arXiv:2110.10610 [gr-qc].
- [60] G. S. Adkins and J. McDonnell, *Phys. Rev. D* **75**, 082001 (2007), arXiv:gr-qc/0702015 [gr-qc].
- [61] S. Benczik, L. N. Chang, D. Minic, N. Okamura, S. Rayyan, and T. Takeuchi, *Phys. Rev. D* **66**, 026003 (2002), arXiv:hep-th/0204049 [hep-th].
- [62] L. Iorio, *Int. J. Mod. Phys. D* **24**, 1530015-343 (2015), arXiv:1412.7673 [gr-qc].
- [63] L. Iorio, *Astrophys. J.* **157**, 220 (2019), arXiv:1810.13415 [gr-qc].
- [64] GRAVITY Collaboration, *Astron. Astrophys.* **636**, L5 (2020), arXiv:2004.07187 [astro-ph.GA].
- [65] E. Deligianni, B. Kleihaus, J. Kunz, P. Nedkova, and S. Yazadjiev, *Phys. Rev. D* **104**, 064043 (2021).
- [66] I. Banerjee, *J. Cosmol. Astropart. Phys.* **2022**, 034 (2022).
- [67] D. Foreman-Mackey, D. W. Hogg, D. Lang, and J. Goodman, *Publ. Astron. Soc. Pac.* **125**, 306 (2013), arXiv:1202.3665 [astro-ph.IM].
- [68] R. A. Remillard and J. E. McClintock, *Annu. Rev. Astron. Astrophys.* **44**, 49 (2006), arXiv:astro-ph/0606352 [astro-ph].
- [69] A. A. Molla, S. K. Chakrabarti, D. Debnath, and S. Mondal, *Astrophys. J.* **834**, 88 (2017), arXiv:1611.01266 [astro-ph.HE].
- [70] A. Ingram and S. Motta, *Mon. Not. R. Astron. Soc.* **444**, 2065 (2014), arXiv:1408.0884 [astro-ph.HE].
- [71] R. A. Remillard, M. P. Muno, J. E. McClintock, and J. A. Orosz, *Astrophys. J.* **580**, 1030 (2002), arXiv:astro-ph/0202305 [astro-ph].
- [72] J. A. Orosz, J. F. Steiner, J. E. McClintock, M. A. P. Torres, R. A. Remillard, C. D. Bailyn, and J. M. Miller, *Astrophys. J.* **730**, 75 (2011), arXiv:1101.2499 [astro-ph.SR].
- [73] S. E. Motta, T. M. Belloni, L. Stella, T. Muñoz-Darias, and R. Fender, *Mon. Not. R. Astron. Soc.* **437**, 2554 (2014), arXiv:1309.3652 [astro-ph.HE].